DYNAMICS OF THE WEDDEL SEA ANOMALY AND MAIN IONOSPHERIC TROUGH IN THE SOUTHERN SUMMER HEMISPHERE

© 2025 A. T. Karpachev

Pushkov Institute of Terrestrial Magnetism, Ionosphere and Radio Wave Propagation of the Russian Academy of Sciences (IZMIRAN), Moscow, Troitsk, Russia

e-mail: karp@izmiran.ru

Received May 31, 2024
Revised July 16, 2024
Accepted July 25, 2024

Abstract. The impact of the Weddell Sea Anomaly on the structure of the nighttime ionosphere in the Southern summer hemisphere is considered in detail. For this purpose, data from the CHAMP satellite were used in January 2003 under high solar activity and in January 2008 under low solar activity. The data relate to the local time interval 02–04 LT, when the increase in electron density due to the formation of an anomaly is the strongest. At longitudes of 60–180° E under high solar activity and 0-210° E at low solar activity, where there is no anomaly, the main ionospheric trough is observed. The plasma peak in the nighttime ionosphere associated with the anomaly formation reaches 6 MHz under low solar activity, and 10 MHz under high solar activity. The strongly developed plasma peak decreases sharply to high latitudes at the equatorward border of auroral diffuse precipitation, which corresponds to the plasmapause. When the anomaly is weakly developed, the contribution of diffuse precipitation becomes noticeable, so that the plasma peak expands towards the pole due to these precipitation. Poleward of anomaly, the high-latitude trough is usually observed at latitudes of the auroral oval. A well-defined minimum of the electron density is often formed equatorward of Weddell Sea Anomaly, which can be defined as a sub-trough. Sometimes the sub-trough is created by the escape of ionospheric plasma from the summer hemisphere to the winter hemisphere. Then a density maximum is formed in the winter hemisphere at conjugate latitudes. Sub-trough is much more common under low solar activity than under high activity.

DOI: 10.31857/S00167940250607e5

1. INTRODUCTION

At the ionospheric stations Halley Bay (75.6° S, 333.4° E, 65.8° GMLat) and Argentine Island (65.3° S, 295.7° E, 53.8° GMLat), the anomalous behavior of *foF2* was first detected: at the time of

the December solstice, the night values strongly exceed the day values [Bellchambers and Piggott, 1958; Penndorf, 1965; Dudeney and Piggot, 1978]. This effect was named the Weddell Sea Anomaly (WSA) after the name of the nearest sea. Studies of WSA characteristics were later continued using data from the TOPEX/Poseidon experiment for all levels of solar activity and all seasons [Horvath and Essex, 2003; Horvath, 2006; Jee et al, 2009], from direct measurements of *Ni* ion concentration at the DMSP satellite altitude of 850 km [Horvath and Lovell, 2009] and *Ne* electron concentration at the CHAMP satellite altitude of 400 km [Liu et al., 2010], as well as from radio occultation measurements in the COSMIC/Formosat experiment [Burns et al., 2008; He et al., 2009; Lin et al., 2009]. The anomaly region was clearly delineated using data from the Intercosmos-19 and CHAMP satellites in [Karpachev et al., 2011 and Klimenko et al., 2015]. In all the cited works, the causes of anomaly formation were also discussed. A detailed study of the mechanism of anomaly formation using ground station data and the FLIP model was carried out in a recent paper [Richards et al., 2018]. The main reason for the strong increase of the electron concentration at night at the latitudes of the anomaly is the action of the neutral wind in the presence of high residual ionization after "switching off" the solar radiation.

The main ionospheric failure (MIF) was discovered and described in the pioneering work of Muldrew [1965]. In addition to the MIG, Muldrew observed another failure at higher latitudes, which he defined as a high-latitude ionospheric failure (HLF). Both failures have been repeatedly investigated, with results presented in reviews [Ahmed et al., 1979; Moffett and Quegan, 1983; Grebowsky et al., 1983; Williams and Jain, 1986; Rodger et al., 1992; Nilsson et al., 2005]. As both failures were investigated, VIP was found to be located within the auroral oval of the rash [Grebowsky et al., 1983], while ISU was predominantly located equatorially above the oval [Ahmed et al., 1979]. However, VIP located at the lowest latitude possible can be confused with ISU, which is located at the highest latitude possible. Therefore, a special method using the auroral oval model has been proposed to separate the VIP and the ISU [Vorobjev et al., 2013]. This model was developed using DMSP satellite data at the Polar Geophysical Institute in Murmansk and is available at http://apm.pgia.ru. The model describes the zone I auroral diffuse melt at the equatorial edge of the auroral oval and zone II diffuse melt at its polar edge. It was shown that zone I usually forms the polar wall of the ISU, while zone II forms the polar wall of the VIP. This is a key factor in distinguishing the ISU from the VIP. The analysis is most effective in the framework of the longitude effect, since the position of all ionospheric structures depends on longitude. The position of the auroral oval also depends on longitude and is determined by the angle of inclination of the Earth's dipole [Karpachev, 2023]. The amplitude of longitudinal variations of the auroral oval of rashes is ~2.5°.

ISU is most pronounced in winter night conditions. However at night, it is sufficiently well manifested in summer as well. In the summer Southern Hemisphere, the failure dynamics should be strongly affected by the Weddell Sea anomaly. To verify this assumption is the purpose of this study.

2. DATA

Data from direct measurements of electron *Ne* concentration on the CHAMP satellite [Rother and Michaelis, 2019] were used in this work. The data were sampled for on January 05–11, 2003 at high solar activity (*F10*.7~160 sfu) and for on January 03–13, 2008 at low solar activity (*F10*.7~80 sfu). The data refer to relatively quiet time periods with $Kr \leq 4$. The satellite orbited in a nearly polar orbit with an inclination of 87°, the orbital altitude was ~ 520 km in January 2003 and ~ 360 km in January 2008. The variations of *Ne* are presented below in terms of the plasma frequency *fp*. Measurements were made at ~1° latitude intervals, which allows for a reasonably accurate determination of the positions of all ionospheric structures. The CHAMP satellite data are freely available online (https://isdc.gfz-potsdam.de/champ-isdc/).

3. DISTRIBUTION OF ELECTRON CONCENTRATION IN THE SOUTHERN HEMISPHERE

Fig. 1.

Fig. 1 shows the Southern Hemisphere *fp* distribution for 02– 04 LT obtained from CHAMP data for high solar activity (HSA) and low solar activity (LSA). The maps are derived from data for several quiet days in January 2003 and January 2008, respectively. The *fp* values are much higher under WSA than under NSA, although the satellite was closer to the maximum of the *F2* layer under low activity. However, the two distributions are similar in structure. In both cases, there is a strong increase in electron concentration associated with WSA formation: at longitudes from 180° W to 70° Å at WSA, and from 150° W to 70° Å at NSA. The anomaly is much more strongly developed at WSA. The dashed curve shows the ISU position determined for 04 LT, but under winter conditions. Due to data averaging, the summer ISU is clearly shown on the maps only at longitudes 90–150° Å at WSA and at longitudes 60–210° Å at NSA. The VIP is clearly manifested only at longitudes 120–180° Å at WSA. Thus, a comparison of the electron concentration distributions for high and low solar activity reveals both similarities and differences between the two. More subtle differences will be identified and discussed below in the detailed analysis.

4. VARIATIONS OF DIFFERENT STRUCTURES IN THE SOUTHERN HEMISPHERE AT HIGH SOLAR ACTIVITY

Fig. 2.

Fig. 3.

Fig. 2 shows the longitude variations of different structures of the summer nighttime ionosphere in the Southern Hemisphere. CHAMP satellite data for the WSA obtained January 06–10, 2003 were used. Fig. 3 shows the latitude profiles of *fp* obtained at different longitudes on January 7, 2003 for quiet geomagnetic conditions (*Kp* varied from 1+ to 3-). The data in the region of middle and high latitudes refer to the post-midnight ionosphere in the interval 02–04 LT. The areas of auroral diffuse precipitations are shaded in Fig. 2.

The asterisks in Fig. 2 show the position of the *Ne* peak associated with the WSA. The vertical lines show the width of this peak, but only for 07 January so as not to clutter the graph. The filled circles in Fig. 2 indicate the position of the ISU. The ISU is understood as a structure corresponding to the classical main ionospheric failure, i.e. a sufficiently deep minimum of electron concentration at typical latitudes of the ISU and a polar wall at the latitudes of precipitation in the zone I. The polar wall of the ISU is indicated by triangles. Polar high-latitude dip is often observed above the ISU, it is indicated by empty circles. The VIP is usually observed inside the auroral oval, its polar wall is formed by diffuse rashes in zone II. Fig. 2 shows that the classical ISU is clamped by the WSA in longitude on both sides, so that it is observed only in the longitude interval 60–180° E. Actually, this is the main feature of the nighttime summer ionosphere of the Southern Hemisphere. The thick curve shows the position of the winter ISU also for 04 LT [Karpachev et al., 2019]. It can be seen that the positions of the summer and winter dips do not differ significantly. At low longitudes, the ISU transforms into a structure that resembles a failure, but its minimum is located much lower in latitude than the classical ISU and, correspondingly, the equatorial edge of the auroral oval. Let us define this structure as a sub-oval. The sub-ovals are indicated by squares in Fig. 2. They are observed in Fig. 3 at turns, which correspond to longitudes 50, 26, and 3° E. The transition of the ISU into a subwavelength occurs so imperceptibly that it is easy to miss when analyzing it. For example, the structure at longitude 60° E in Fig. 3 can be interpreted in two ways, both as an ISU and as a subwarp. At this transition, the polar wall of the ISU as at longitude 84° Å also passes imperceptibly into the plasma peak at longitude 50° Å, already clearly associated with the WSA. It follows from the above that the structure of the ISU/subproval can be unambiguously identified only in dynamics, considering the whole picture as a whole, as in Fig. 2.

WSA begins to develop at longitudes less than 60° Å. At the equatorial edge of the anomaly, a sub-peninsula is usually formed. With further decrease of the observational longitude, it becomes less and less noticeable and disappears at the transition to the Western Hemisphere. The WSA in the

Western Hemisphere is the dominant structure, in Fig. 2 it is limited to the latitude – 40°, in fact it extends further to the equator, but in this case it is not fundamental. The high-latitude edge of the WSA in the Western Hemisphere coincides surprisingly precisely with the equatorial boundary of Zone I. However, this is quite natural, since the rash boundary almost coincides with the plasma pause. The polar wind outside the plasma pause carries the ionospheric plasma along the geomagnetic field lines upward and further to the magnetosphere. Therefore, the polar boundary of the WSA is very sharp. Then the electron concentration decreases slowly and forms the WSA minimum. Its polar wall is formed by rashes in zone II. At low longitudes in the Eastern Hemisphere, the WSA is bounded not by the equatorial but by the polar boundary of zone I. This is explained by the fact that at these longitudes the WSA is just beginning to form, so that at low background levels the effect of rashes becomes noticeable. In other words, in this case, the polar edge of the plasma peak is formed by diffuse rashes.

The VIP is a very variable structure, both in shape and position, so it is virtually unreproducible in data averaging and is reflected on the map only in the longitude range 120–180° E. Similarly, the subprovals are reflected on the map together with the ISU only in the longitude interval 30–75° E.

The dynamics of dips and WSA in the summer Southern Hemisphere is so complex that it leads to contradictory results in its study. For example, in [Aa et al., 2020], statistical processing of Swarm satellite data showed that the Southern Hemisphere summer dip is on average located 1.4° equatorial to the winter dip. In [Yang et al., 2018)], the summer ISU was identified, as one would expect, only in the longitude interval 60–90° Å, but it was on average 3° equatorial than the winter failure. This is obviously due to the fact that in both cases the data set also included a subprovals, which underestimated the average position of the ISU. In [Lee et al., 2011], data from the COSMIC/Formosat experiment were considered only outside the WSA, but the mean position of the 04 LT failure turned out to be much more polar than the winter ISU, at latitudes 64–65°. It is not difficult to determine in Figure 2 that this corresponds to the VIP, not the ISU.

In Fig. 3 shows the latitude profiles of *fp* obtained at different longitudes on January 7, 2003. They were practically discussed in the process of describing Fig. 2. Note again how smoothly the plasma peak forming the polar wall of the ISU is absorbed by the plasma peak in the formation of the WSA. Let us note one more feature in Fig. 3. In the lowest *fp* profile obtained at longitude 212° Å, the electron concentration slowly decreases toward high latitudes, forming a shallow WIP with a very low polar wall. Such latitude profiles are typical in the longitude interval 150–250° Å. The VIP in this longitude interval is maximally distant to the pole. This is probably related to the specificity of the eruptions in Zone II in this longitude interval.

Fig. 4.

For a more complete understanding of the morphology and causes of the formation of the nighttime summer ionosphere of the Southern Hemisphere, let us consider the most characteristic latitudinal sections of *fp* - Fig. 4. In Fig. 4*a* shows in comparison two sections - in the normal and anomalous ionosphere. The sections were obtained on January 9, 2003 in longitude sectors 105° Å and 335° Å. At longitude 105° Å, a classical ISU is observed in the normal ionosphere, the polar wall of which is formed by rashes in zone I. The ISU is also accompanied by a well-defined VIP, the polar wall of which is correspondingly formed by rashes in zone II. The positions of the eruption zones correspond to the longitude of observations and the Kr-index. In the anomalous ionosphere, an extremely strongly pronounced increase of the electron concentration associated with the formation of WSA is observed. This increase reaches 9–10 MHz at its maximum. The plasma peak is sharply cut off at the latitude of the plasma pause, the WSA minimum is observed somewhat more polar and its polar wall is located even farther in latitude. Thus, the WSA completely absorbs the ISU but does not affect the VIP, at least not strongly.

In Fig. 4*b* shows an extremely characteristic latitudinal *fp* profile obtained on January 13, 2003 at longitude 22° Å and a conjugate *fp* profile recorded in the Northern Hemisphere for almost the same conditions (dashed curve). In the Northern Hemisphere, a classical ISU is observed with a minimum at latitude 62°. In the Southern Hemisphere, a plasma peak associated with the WSA begins to form at the failure latitude, at the same longitude 22° E. This peak is not powerful enough to completely engulf the ISU, but it shifts the ISU minimum toward the pole. This minimum is marked with a circle in Fig. 4. And equatorward of the WSA a subprovolution is formed at latitude −50.5°, which is marked with a square. Note that no specific mechanism for the formation of the subpeninsula was not involved - the minimum of the electron concentration is formed simply because the concentration grows both toward the equator and the pole.

Fig. 4*c* also shows the *fp* profiles in the Southern and conjugate Northern Hemisphere. In the Northern Hemisphere, the ISU is located at latitude 58°, which corresponds to longitude and *Kr*. In the Southern Hemisphere, an anomaly begins to form at longitude 47° E that fills the ISU minimum. Instead, a shallow minimum is formed, marked by a square. This minimum is located at latitude −52°, which is too low for the ISU, so it is a sub-roval. In the conjugate Northern Hemisphere, a small peak in electron concentration is observed at these latitudes. The mechanism of formation of such a conjugate structure is well known - from the summer hemisphere with an increased level of ionization, the plasma along the magnetic force tube flows to the winter hemisphere due to diffusion [Krinberg and Tashchilin, 1984]. This mechanism is most effective for middle latitudes, where the volume of power tubes maximally contributes to the process of ionospheric plasma flow.

Fig. 4*d* also shows the conjugate profiles of *fp* obtained on January 8, 2003 in the longitude sector ~35° Å. In the Northern Hemisphere, a well-defined ISU is observed. In the Southern Hemisphere, the WSA completely fills the ISU. And at very low latitudes -(43– 47°) a minimum is observed, again conjugated with the plasma peak in the Northern Winter Hemisphere.

Thus, we can distinguish two reasons for the formation of the subproval, which is observed quite regularly in the longitude interval 0–60° E. One of them is connected with the pumping of plasma from the summer hemisphere to the winter hemisphere under the action of diffusion. The second reason is due to the sharp growth of the electron concentration toward the pole during the formation of the WSA, and in the presence of the concentration growth toward the equator. In turn, the concentration growth toward the equator is associated either with the equatorial anomaly crest or with the local *Ne* maximum at low latitudes, which is usually observed even after the equatorial anomaly decay [Karpachev, 2021].

5. VARIATIONS OF DIFFERENT STRUCTURES IN THE SOUTHERN HEMISPHERE AT LOW SOLAR ACTIVITY

Fig. 5.

Let us consider the situation in the Southern Hemisphere at low solar activity and highlight its differences from high solar activity. Fig. 5 shows the longitudinal variations of structures of the Southern Hemisphere isolated for the period January 03–11, 2008 for the NSA and quiet geomagnetic conditions. The data refer to almost the same local time interval as in Figure 2 (03– 04 LT). In Fig. 6 shows the latitudinal profiles of *fp* characteristic of the NSA. Fig. 6*a*, similar to Fig. 4*a*, shows the latitudinal profiles in the normal and anomalous ionosphere. At NSA, the increase in electron concentration at night in the WSA region reaches only 6 MHz compared to 10 MHz at WSA. The ISU, on the contrary, is more pronounced at NSA. Therefore, the region of existence of the classical ISU at NSA is wider than at WSA and occupies the longitude interval 0–225° Å, as can be seen in Fig. 5. The weaker development of WSA also affects the fact that the polar boundary of all plasma peaks in Fig. 5 is defined by diffuse rashes, and not only at low longitudes as in WSA (Fig. 2). This is due to the fact that the effect of rashes becomes more prominent at low background levels.

However, the main difference from WSA is the presence of subbands in the Western Hemisphere. Moreover, the subpeninsulas are observed at much lower latitudes than in WSA. Two examples of sub-provals are shown in Fig. 6*b*. The sub-wave recorded on January 11, 2008 in longitude sector 25° E at latitude –52°, is similar to the sub-waves observed at low longitudes at WSA. The subproval registered in longitude sector 323° E is located at a very low latitude – 37°.

However, it stands out clearly enough so that it is impossible not to notice it during data processing. Especially, if we are talking about automatic extraction of dips. Such a technique has been used more and more often recently. Note that there are no subcavities in the Western Hemisphere at WSA for a simple reason - they are filled due to more intense solar ionization. But even at NSA, the subbands in the Western Hemisphere are not very pronounced.

The triangles in Fig. 5 indicate the position of the polar wall of the ISU formed as a separate peak. The polar wall of the ISU, as usual, is associated with diffuse rashes in zone I. In the longitude interval 120– 210° E, the polar wall is still steep, but there are many plasma peaks at its apex, which makes its position difficult to determine, and it is not marked in Fig. 5.

Fig. 6.

Figure 6*c* is completely similar to Fig. 4*b*. In Fig. 6*c* shows the characteristic latitudinal profile of *fp* obtained on January 05, 2006 at longitude 22° E and the conjugate *fp* profile recorded in the Northern Hemisphere for almost the same conditions. In the Northern Hemisphere, a classical ISU is observed with a minimum at latitude 62°. In contrast, the Southern Hemisphere at these latitudes shows a plasma peak associated with WSA formation. Since the data refer to midnight local time, the WSA is not yet strongly developed and the plasma peak does not fully absorb the ISU. However, this peak shifts the minimum of the ISU toward the pole and also forms a sub-penetration at latitude – 50.5°.

Fig. 6*d* shows the latitude profiles of *fp* obtained on January 5, 2008 in longitude sector 215° E. In the Southern Hemisphere, there is a well-defined sub-provale at latitude – 47°. A plasma peak is observed at the same approximate latitude in the Northern Hemisphere. Thus, the mechanism of plasma pumping from the summer hemisphere to the winter hemisphere works quite effectively also at low solar activity.

In [Horwath and Lowell, 2009], a study of the failure and WSA was carried out using DMSP F15 satellite data for the winter of 1996 − 1997, i.e., also for the NSA. The results obtained can be compared with ours. The plasma pause, ISU, WSA peak and sub-provals from DMSP data were at latitudes – 62.5,– 57.5,– 56.2 and– 42.5° respectively. This is very close to what is observed in Fig. 5. The authors attributed the formation of the subproval to plasma stagnation and the influence of the South Atlantic magnetic anomaly. And displayed in Fig. 6 of their paper, they displayed the ISU and the subproval as a single branch, i.e., they combined completely different structures into one whole. However, the high-latitude edge of the magnetic anomaly barely reaches– 35° GMLat, so it is difficult to agree with its participation in the formation of the subprovals. As for the stagnation of

the ionospheric plasma, it occurs at all latitudes and longitudes in the night ionosphere in the absence of solar ionization.

6. CONCLUSION

The contradictory results obtained for the failure of ionization in the Southern summer hemisphere indicate a situation that is not easy to analyze. A detailed examination of the structure of the summer nighttime (02– 04 LT) ionosphere in the Southern Hemisphere has fully confirmed this assumption. The complex behavior of the ionosphere under these conditions is determined by the Weddell Sea anomaly. Let us emphasize the main provisions of the performed analysis.

– The plasma peak associated with WSA formation in 02–04 LT reaches 6 MHz at NSA and 10 MHz at WSA.

– At WSA longitudes, this peak completely fills the main ionospheric dip. Therefore, the ISU is observed only outside the WSA, at longitudes 60–180° Å at WSA and 0–210° Å at NSA.

– At WSA, the well-developed plasma peak associated with WSA sharply decreases to the pole at the latitude of the plasmapause. This latitude practically coincides with the equatorial boundary of auroral diffuse rashes. At the NSA, the plasma peak associated with the WSA is less strongly developed, so it expands toward the pole at the expense of diffuse rashes in Area I. As a result, the merged peak appears to be limited by the latitude of the polar boundary of the diffuse rashes in Area I. In other words, the polar boundary of the combined peak is determined by the degree of development of the WSA. The boundaries of auroral diffuse eruptions were determined using the auroral oval model [Vorobjev et al., 2013].

– At the equatorial boundary of the plasma peak of the WSA, a sub-penetration is often formed at latitudes much more equatorial than the classical ISU, up to ~35° GMLat. At WSA, this subproval is observed only at longitudes in the Eastern Hemisphere 0–60° E, and at NSA and in the Western Hemisphere. The subproval, especially in the Western Hemisphere, is weakly pronounced, is much more equatorial than the ISU, and yet in some papers it is confused with the ISU. Therefore, it cannot be excluded from the analysis.

– There are apparently two reasons for the formation of the subproval. The first and the simplest is that the minimum of the subproval is formed by a sharp increase in electron concentration toward the pole during the formation of the WSA, and toward the equator– in the presence of the equatorial anomaly ridge or its remnants. The second reason is related to the transfer of electron concentration from the summer hemisphere to the winter hemisphere. This mechanism is well known.

ACKNOWLEDGEMENTS

The author thanks the developers and operators of the CHAMP experiment (Deutsches GeoForschungs Zentrum (GFZ)) and the German Aerospace Center (DLR) for providing the data. CHAMP data are from https://isdc.gfz-potsdam.de/champ-isdc/.

REFERENCES

1. *Krinberg I.A., Tashchilin A.V.* Ionosphere and plasmasphere. M.: Nauka, 189 p. 1984.

2. *Karpachev A.T., Gasilov N.A., Karpachev O.A.* Morphology and causes of the Weddell Sea anomaly // Geomagnetism and Aeronomy. V. 51. No. 6. P. 828−840. 2011.

3. *Karpachev A.T.* Daily and longitudinal variations of the equatorial anomaly for the winter solstice according to the Intercosmos-19 satellite // Geomagnetism and Aeronomy. V. 61. No. 1. P. 20−34. 2021. https://doi.org/10.31857/S0016794021010065

4. *Karpachev A.T.* Features of the structure of the winter morning ionosphere of high and middle latitudes // Geomagnetism and Aeronomy. V. 63. No. 6. P. 788–797. 2023. https://doi.org/10.31857/S0016794023600370

5. *Aa E., Zou S., Erickson P. J., Zhang S.-R., Liu S.* Statistical analysis of the main ionospheric trough using Swarm in situ measurements // J. Geophys. Res. – Space. V. 125. N 3. ID e2019JA027583. 2020. https://doi.org/10.1029/2019JA027583

6. *Ahmed M., Sagalyn R.C., Wildman P.J.L., Burke W.J.* Topside ionospheric trough morphology: occurrence frequency and diurnal, seasonal and altitude variations // J. Geophys. Res. – Space. V. 84. N 2. P. 489–498. 1979. https://doi.org/10.1029/JA084iA02p00489

7. *Bellchambers W.H., Piggott W.R.* Ionospheric measurements made at Halley Bay // Nature. V. 182. N 4649. P. 1596–1597. 1958. https://doi.org/10.1038/1821596a0

8. *Burns A.G., Zeng Z., Wang W., Lei J., Solomon S.C., Richmond A.D., Killeen T.L., Kuo Y.-H.* The behavior of the *F*2 peak ionosphere over the South Pacific at dusk during quiet summer conditions from COSMIC data // J. Geophys. Res. – Space. V. 113. N 12. ID A12305. 2008. https://doi.org/10.1029/2008JA013308

9. *Dudeney J.R., Piggott W.R.* Antarctic ionospheric research / Upper Atmosphere Research in Antarctica / Antarctic Research Ser., 29. Eds. L.J. Lanzerotti, C.G. Park. Washington, DC: American Geophysical Union. P. 200–235. 1978. https://doi.org/10.1029/AR029p0200

10. *Grebowsky J.M., Tailor H.A., Lindsay J.M.* Location and source of ionospheric high latitude troughs // Planet. Space Sci. V. 31. N 1. P. 99–105. 1983. https://doi.org/10.1016/0032-0633(83)90034-X

11. *He M., Liu L., Wan W., Ning B., Zhao B., Wen J., Yue X., Le H.* A study of the Weddell Sea Anomaly observed by FORMOSAT-3/COSMIC // J. Geophys. Res. – Space. V. 114. N 12 ID A12309. 2009. https://doi.org/10.1029/2009JA014175

12. *Horvath I., Essex E.A.* The Weddell Sea Anomaly observed with the TOPEX satellite data // J. Atmos. Sol. Terr. Phys. V. 65. N. 6. P. 693–706. 2003. https://doi.org/10.1016/S1364-6826(03)00083-X.

13. *Horvath I.* A total electron content space weather study of the nighttime Weddell Sea Anomaly of 1996/1997 southern summer with TOPEX/Poseidon radar altimetry // J. Geophys. Res. – Space. V. 111. N 12. ID A12317. 2006. https://doi.org/10.1029/2006JA011679

14. *Horvath I., Lovell B.C.* Investigating the relationships among the South Atlantic Magnetic Anomaly, southern nighttime midlatitude trough, and nighttime Weddell Sea Anomaly during southern summer // J. Geophys. Res. – Space. V. 114. N 2. ID A02306. 2009. https://doi.org/10.1029/2008JA013719

15. *Jee G., Burns A.G, Kim Y.-H., Wang W.* Seasonal and solar activity variations of the Weddell Sea Anomaly observed in the TOPEX total electron content measurements // J. Geophys. Res. – Space. V. 114. N 4. ID A04307. 2009. https://doi.org/10.1029/2008JA013801

16. *Karpachev A.T., Klimenko M.V., Klimenko V.V.* Longitudinal variations of the ionospheric trough position // Adv. Space Res. V. 63. N 2. P. 950–966. 2019. https://doi.org/10.1016/j.asr.2018.09.038

17. *Klimenko M.V., Klimenko V.V., Karpachev A.T., Ratovsky K.G., Stepanov A.E.* Spatial features of Weddell Sea and Yakutsk Anomalies in *foF*2 diurnal variations during high solar activity periods: Interkosmos-19 satellite and ground-based ionosonde observations, IRI reproduction and GSM TIP model simulation // Adv. Space Res. V. 55. N 8. P. 2020–2032. 2015. https://doi.org/10.1016/j.asr.2014.12.032

18. *Lee I.T., Wang W., Liu J.Y., Chen C.Y., Lin C.H.* The ionospheric midlatitude trough observed by FORMOSAT-3/COSMIC during solar minimum // J. Geophys. Res. – Space. V. 116. N 6. ID A06311. 2011. https://doi.org/10.1029/2010JA015544

19. *Liu H., Thampi S.V., Yamamoto M.* Phase reversal of the diurnal cycle in the midlatitude ionosphere // J. Geophys. Res. – Space. V. 115. N 1. ID A01305. 2010. https://doi.org/10.1029/2009JA014689

20. *Lin C.H., Liu J.Y., Cheng C.Z., Chen C.H., Liu C.H., Wang W., Burns A.G., Lei J.* Three-dimensional ionospheric electron density structure of the Weddell Sea Anomaly // J. Geophys. Res. – Space. V. 114. N 2. ID A02312. 2009. https://doi.org/10.1029/2008JA013455

21. *Moffett R.J., Quegan S.* The mid-latitude trough in the electron concentration of theionospheric *F*-layer: A review of observations and modeling // J. Atmos. Terr. Phys. V. 45. N 5. P. 315–343. 1983. https://doi.org/10.1016/S0021-9169(83)80038-5

22. *Muldrew D.B. F*-layer ionization troughs deduced from Alouette data // J. Geophys. Res. V. 70. N 11. P. 2635–2650. 1965. https://doi.org/10.1029/JZ070i011p02635

23. *Nilsson H., Sergienko T.I., Ebihara Y., Yamauchi M.* Quiet-time mid-latitude trough: influence of convection, field-aligned currents and proton precipitation // Ann. Geophys. V. 23. N 10. P. 3277–3288. 2005. https://doi.org/10.5194/angeo-23-3277-2005

24. *Penndorft R.* The average ionospheric conditions over the Antarctic / Geomagnetism and Aeronomy: Studies in the Ionosphere, Geomagnetism and Atmospheric Radio Noise / Antarctic Research Ser., 4. Ed. A.H.Waynick. Washington, DC: American Geophysical Union. P. 1–45. 1965. https://doi.org/10.1029/AR004p0001

25. *Richards P.G., Meier R.R., Chen S., Dandenault P.* Investigation of the causes of the longitudinal and solar cycle variation of the electron density in the Bering Sea and Weddell Sea anomalies // J. Geophys. Res. – Space. V. 123. N 9. P. 7825–7842. 2018. https://doi.org/10.1029/2018JA025413

26. *Rodger A.S., Moffett R.J, Quegan S.* The role of ion drift in the formation of ionisation troughs in the mid-and high-latitude ionosphere – a review // J. Atmos. Terr. Phys. V. 54. N 1. P. 1–30. 1992. https://doi.org/10.1016/0021-9169(92)90082-V

27. *Rother M., Michaelis I.* CH-ME-2-PLPT - CHAMP Electron density and temperature time series in low time resolution (Level 2). GFZ Data Services. 2019. https://doi.org/10.5880/GFZ.2.3.2019.007

28. *Vorobjev V.G., Yagodkina O.I., Katkalov Yu.V.* Auroral Precipitation Model and its applications to ionospheric and magnetospheric studies // J. Atmos. Sol.-Terr. Phy. V. 102. P. 157–171. 2013. http://dx.doi.org/10.1016/j.jastp.2013.05.007

29. *Williams P.J.S., Jain A.R.* Observations of the high latitude trough using EISCAT // J. Atmos. Terr. Phys. V. 48. N 5. P. 423–434. 1986. https://doi.org/10.1016/0021-9169(86)90119-4

30. *Yang N., Le H., Liu L., Zhang R.* Statistical behavior of the longitudinal variations of the evening topside mid-latitude trough position in both northern and southern hemispheres // J. Geophys. Res. – Space. V. 123. N 5. P. 3983–3997. 2018. https://doi.org/10.1029/2017JA025048

FIGURE CAPTIONS

Fig. 1. Distribution of the plasma frequency *fp* from CHAMP satellite data in the Southern Summer Hemisphere in January 2003 and January 2008. Local time 02− 04 h. The dashed curve shows the position of the ISU minimum for 04 LT in winter conditions.

Fig. 2. Longitude variations from CHAMP data for high solar activity in January 2003 of the positions of the VIP (empty circles), ISU (filled circles), the polar wall of the ISU (triangles), the subprovals (squares), and the WSA peak (asterisks). Areas I and II of auroral diffuse rashes according to the model [Vorobjev et al., 2013] are shaded. Vertical lines represent the WSA for January 07. Local time 02− 04 h. The thick curve shows the ISU position for 04 LT but under winter conditions.

Fig. 3. Latitude sections of *fp* in different longitude sectors derived from CHAMP data on January 07, 2003. Filled circles are the ISU position, empty circles are the VIP position, and squares are the sub-province position. For convenience, the corresponding longitude sectors are indicated on the left for the three Y axes.

Fig. 4. Characteristic latitude transects of *fp* for different conditions in the Southern and Northern Hemispheres. The date, local time, longitude, and *Kr*-index are given for each case. The dashed curves refer to the Northern Hemisphere. The position of the ISU is indicated by a filled circle, the VIP by an empty circle, and the subproval by a square.

Fig. 5. Longitude variations from CHAMP data for low solar activity in January 2008 of the position of the VIP (empty circles), the ISU (filled circles), the polar wall of the ISU (triangles), the subproval (squares), and the WSA peak (asterisks). Vertical lines represent the WSA for January 10. Zones I and II of auroral diffuse rashes according to the model [Vorobjev et al., 2013] are shaded. Local time is 03− 04 h. The thick curve shows the position of the ISU for 04 LT, but under winter conditions.

Fig. 6. Characteristic latitude transects of *fp* for different conditions in the Southern and Northern Hemispheres. For each case, the date, local time, longitude, and Kr-index are given. The dashed curves refer to the Northern Hemisphere. The position of the ISU is indicated by a filled circle, the VIP by an empty circle, and the subproval by a square.

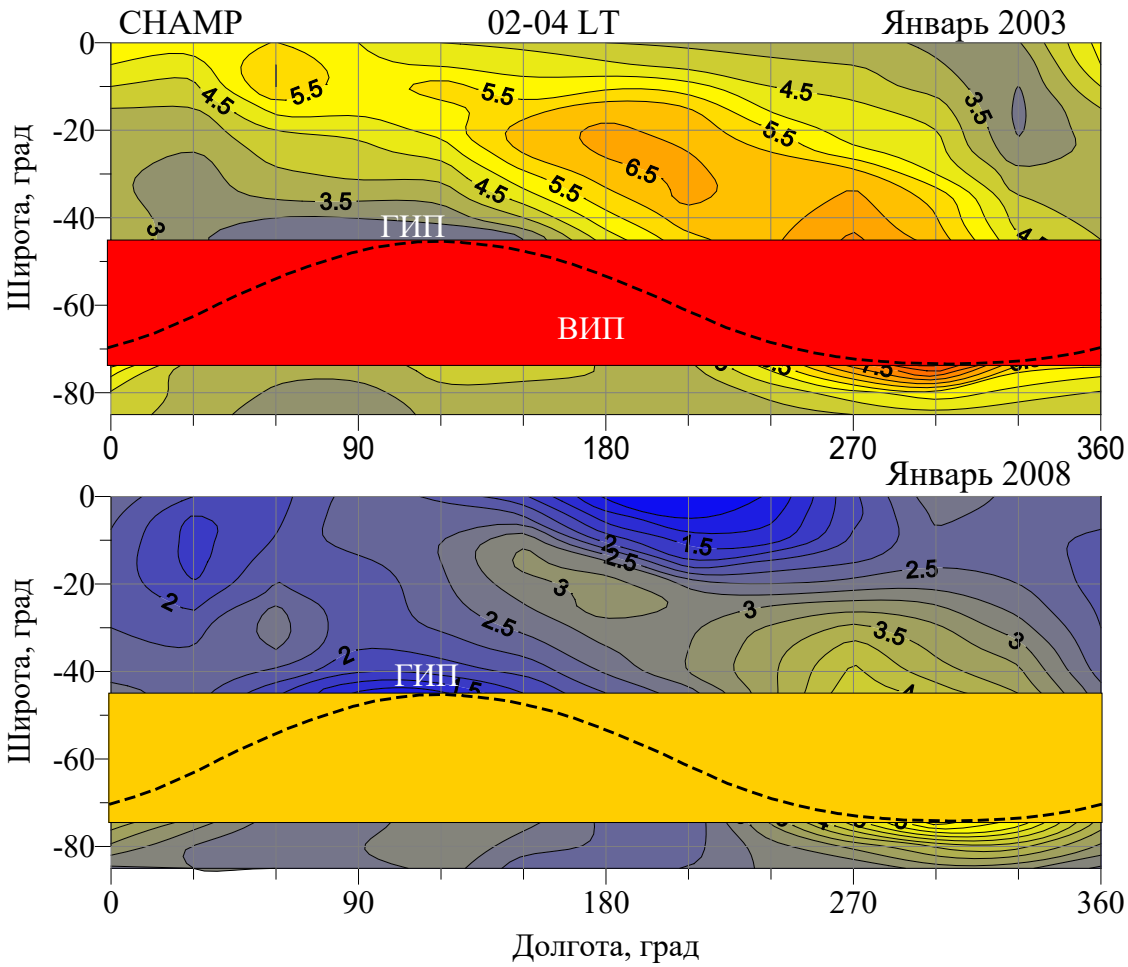
CHAMP
02-04 LT
Январь 2003
Широта, град
ГИП
ВИП
Январь 2008
Широта, град
ГИП
Долгота, град

Fig. 1.

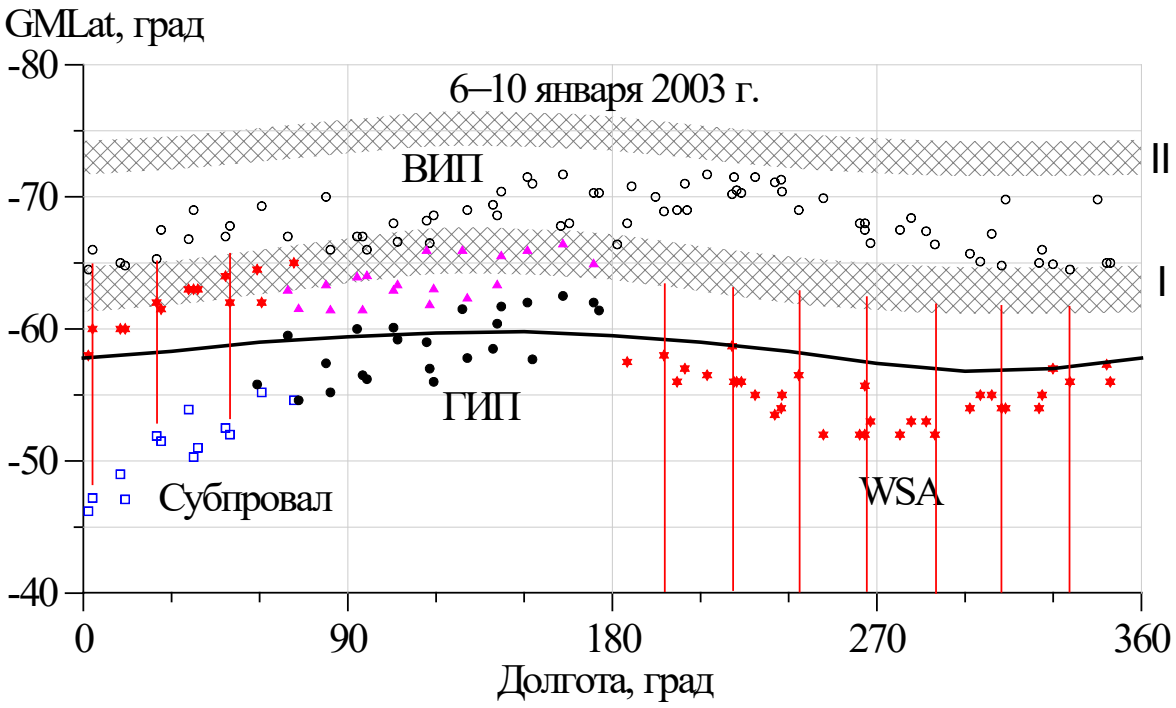
GMLat, град
-80
-70
-60
-50
-40
6–10 января 2003 г.
ВИП
II
I
ГИП
Субпровал
WSA
0
90
180
270
360
Долгота, град

Fig. 2.

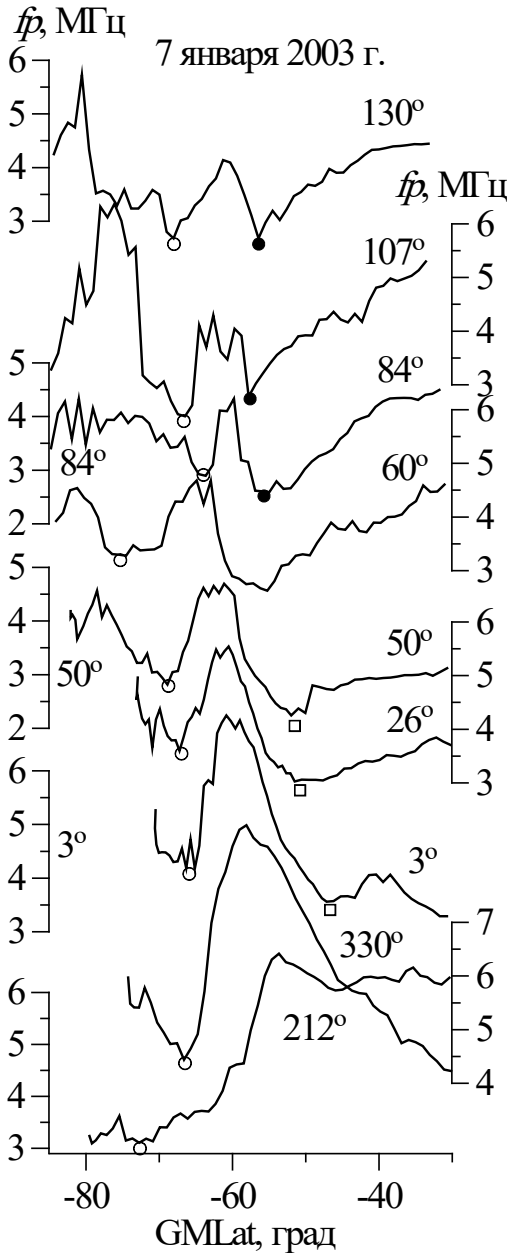
fp, МГц
7 января 2003 г.
130°
fp, МГц
107°
84°
84°
60°
50°
50°
26°
3°
3°
330°
212°
-80
-60
-40
GMLat, град

Fig. 3.

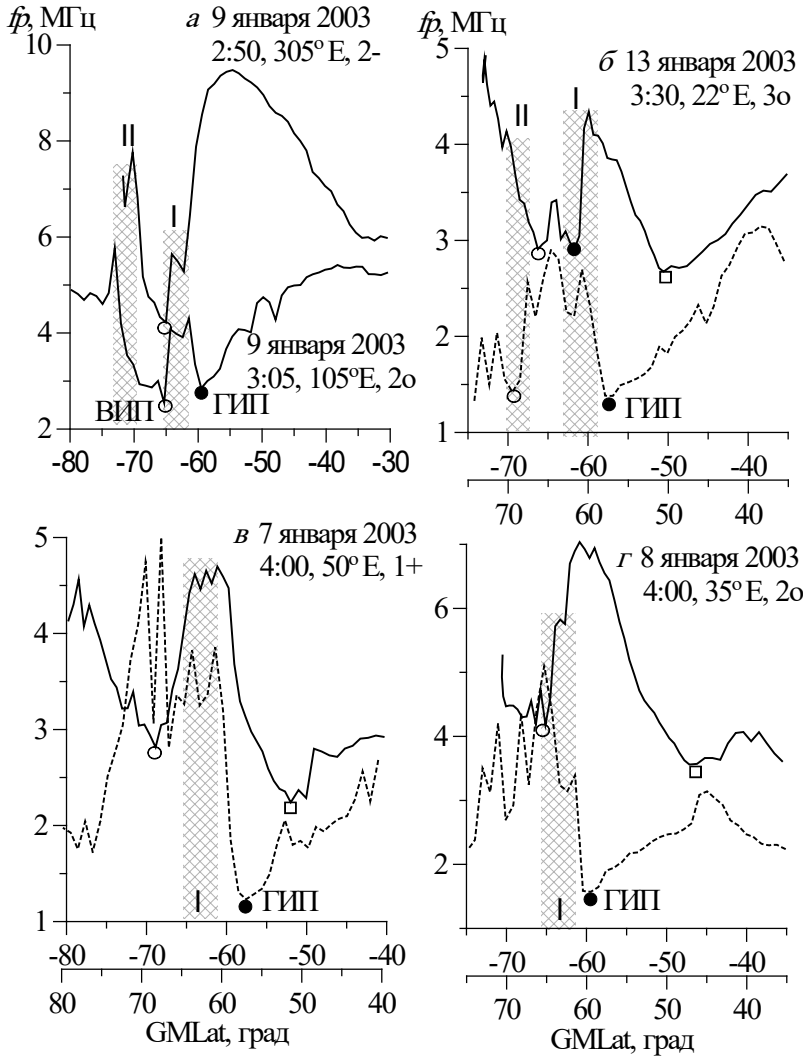
fp, МГц
а 9 января 2003
2:50, 305° E, 2-
II
I
9 января 2003
3:05, 105°E, 2o
ВИП
ГИП
б 13 января 2003
3:30, 22° E, 3o
в 7 января 2003
4:00, 50° E, 1+
г 8 января 2003
4:00, 35° E, 2o
GMLat, град

Fig. 4.

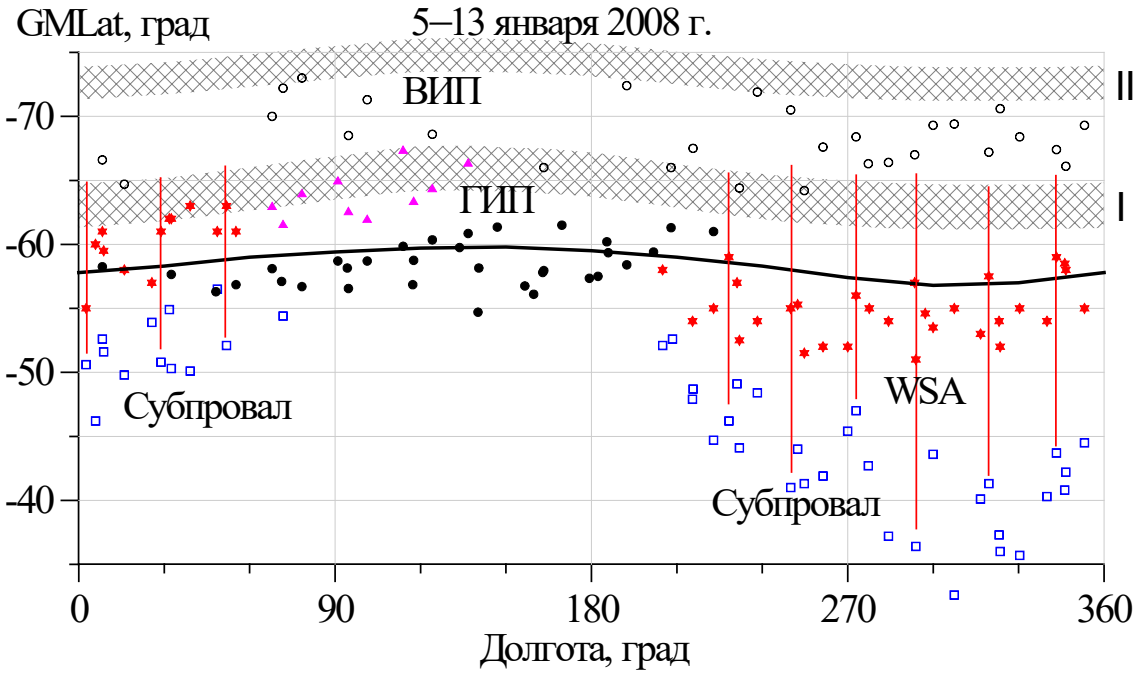
GMLat, град
5–13 января 2008 г.
ВИП
ГИП
II
I
-70
-60
-50
-40
Субпровал
WSA
Субпровал
0
90
180
270
360
Долгота, град

Fig. 5.

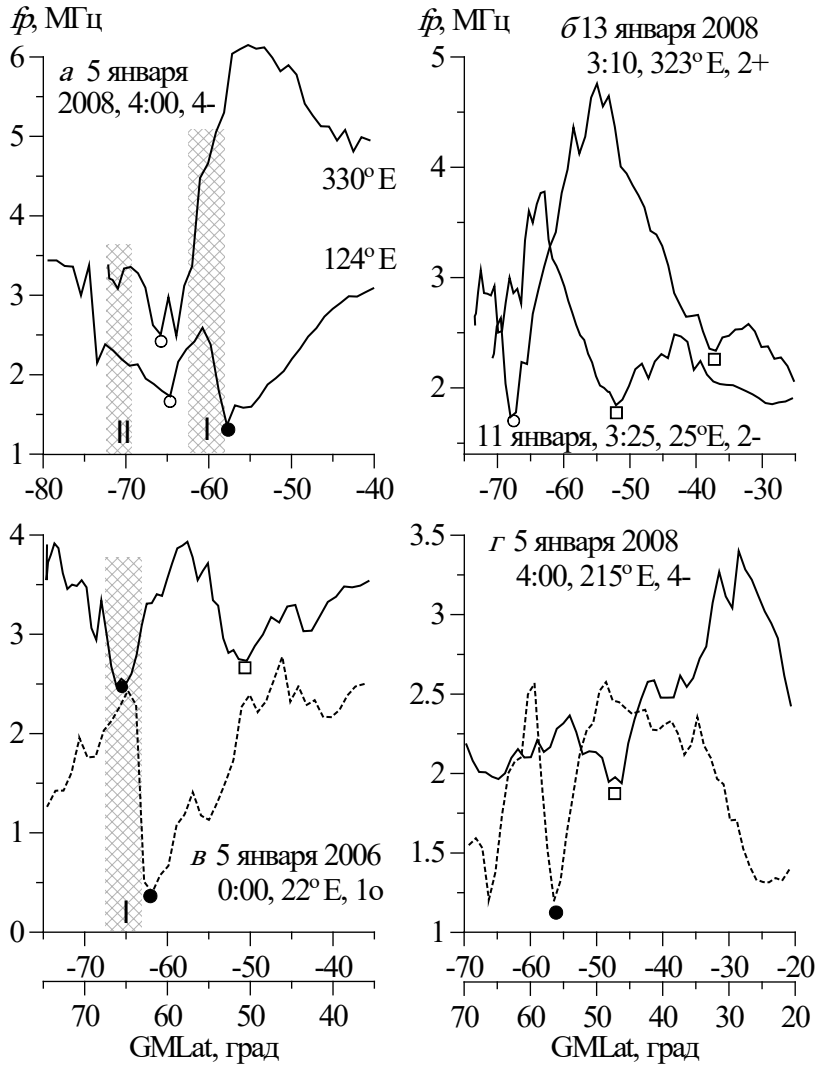
fp, МГц
а 5 января
2008, 4:00, 4-
330° E
124° E
II
I
б 13 января 2008
3:10, 323° E, 2+
11 января, 3:25, 25°E, 2-
в 5 января 2006
0:00, 22° E, 1o
г 5 января 2008
4:00, 215° E, 4-
GMLat, град

Fig. 6.